Pattern bifurcation in the pseudobinary $Ni_3(Al, V)$ alloy: evidence of spontaneous $L1_2$ single crystallization

2002 J. Phys.: Condens. Matter 14 7053

(http://iopscience.iop.org/0953-8984/14/29/307)

INSTITUTE OF PHYSICS PUBLISHING JOURNAL OF PHYSICS: CONDENSED MATTER

J. Phys.: Condens. Matter **14** (2002) 7053–7064 PII: S0953-8984(02)31409-7

Pattern bifurcation in the pseudobinary $Ni_3(Al, V)$ alloy: evidence of spontaneous $L1_2$ single crystallization

M Tanimura[1], **M Kikuchi**[2] **and Y Koyama**[2]

[1] Research Department, Nissan ARC Ltd, 1 Natsushima-cho, Yokosuka, Kanagawa 237-0061, Japan
[2] Kagami Memorial Laboratory for Materials Science and Technology and Department of Materials Science and Engineering, Waseda University, 3-4-1 Ohkubo, Shinjuku, Tokyo 169-0072, Japan

Received 26 February 2002
Published 11 July 2002
Online at stacks.iop.org/JPhysCM/14/7053

Abstract

The structural change between substitution-type ordered structures basically includes the competition of pairwise interactions, which can describe the stability of such structures. The purpose of this study is to investigate the frustration effect resulting from competition related to the $L1_2 \rightarrow D0_{22}$ structural change in the $Ni_3Al_{0.52}V_{0.48}$ alloy and to discuss the pattern bifurcation in the pseudobinary $Ni_3(Al, V)$ alloy. The present data obtained by transmission electron microscopy show that the change in microstructures during the structural change is characterized by the appearance and the subsequent annihilation of $D0_{22}$ regions in the $L1_2$ matrix. The final product of the structural change is the $L1_2$ single phase including topological defects, which is different from the equilibrium state known as the $L1_2 + D0_{22}$ checkerboard pattern. This indicates that the suppression of the $L1_2 \rightarrow D0_{22}$ structural change occurs in this alloy. Such suppression can be explained as being due to an inability to accommodate the strain field in the vicinity of the $L1_2/D0_{22}$ boundaries when $D0_{22}$ precipitation occurs. The trigger of this inability is thought to be strong frustration originating from a small concentration deviation in the initial $L1_2$ matrix from the stoichiometry of the $L1_2$ structure. It is concluded that the formation of the $L1_2$ single phase as the final state, i.e. spontaneous $L1_2$ single crystallization, results from an effort by the alloy to accommodate the strain field, the occurrence of which is related to the frustration effect appearing during the $L1_2 \rightarrow D0_{22}$ structural change.

1. Introduction

Pattern formation is a fascinating theme in statistical physics. In describing the dynamics of pattern bifurcation, a dynamical factor acting as a nonlinear perturbation is important. The

role of such a factor especially attracts our interest when it has a microscopic character such as a topological defect [1]. A phase separation in alloys involving a structural change between substitution-type ordered structures essentially includes such a dynamical factor. Because the stability of an ordered structure can be discussed on the basis of the pairwise interaction [2–4], the diffusion of atoms in the ordered structure results in a high-energy atomic configuration. Thus, the structural change can be regarded as the introduction of the frustration effect between the pairwise interactions that work to stabilize ordered structures. This suggests that the frustration effect becomes a short-range dynamical factor of the phase separation. We have therefore focused on the dynamics of the phase separation, including such structural change, from the viewpoint of pattern bifurcation.

The structural change between ordered structures normally occurs in the eutectoid reaction of intermetallic compounds. The $D0_{19} \rightarrow L1_0$ structural change in the $\alpha(\text{hcp}) \rightarrow \alpha 2(D0_{19}) + \gamma(L1_0)$ eutectoid reaction of the Ti–Al system is one well known example of such structural change. Because the $D0_{19}$ and the $L1_0$ structures are, respectively, A_3B- and AB-type ordered ones, the diffusion of atoms is needed to promote the structural change. In our previous papers, it has been reported that the $D0_{19} \rightarrow L1_0$ structural change in Ti–38–40 at.% Al alloys is characterized by both the appearance and the annihilation of anisotropic lattice-destructed regions under certain conditions [5]. The lattice-destructed regions originate from the vacancies introduced by the deviation from the stoichiometry of the $D0_{19}$ structure, Ti–25 at.% Al. These results indicate that the vacancies play an important role in promoting the structural change and that lattice destruction could become a step to release the frustrated pairwise interaction.

The structural change between the $L1_2$ and the $D0_{22}$ structures is also noteworthy from the viewpoint of the competition between pairwise interactions, although they are A_3B-type ordered structures. Because the $D0_{22}$ structure can be characterized by the periodic array of the antiphase boundaries introduced in the $L1_2$ structure, the stability of both structures has been studied in terms of a long-period superstructure. It has been found that stability can be classified by the number of valence electrons per atom (e/a) [6–9]. Concretely, the $D0_{22}$ structure is stable when e/a is larger than 8.60, while the $L1_2$ structure appears under the condition of e/a smaller than 8.60. This means that the stability of both structures is closely related to the change in the composition of the alloys. In other words, competition between pairwise interactions is presumed to be a key factor in promoting the $L1_2 \Leftrightarrow D0_{22}$ structural change.

A concrete reaction having the $L1_2 \Leftrightarrow D0_{22}$ structural change is the $\gamma(\text{fcc}) \rightarrow \gamma'(L1_2) + \theta(D0_{22})$ eutectoid reaction in pseudobinary $Ni_3(Al, V)$ alloys. According to the phase diagram of the $Ni_3(Al, V)$ alloy system, the $Ni_3Al_{0.2}V_{0.8}$ alloy with $e/a = 8.65$ undergoes the eutectoid reaction at 1281 K [10]. An important feature of the reaction is that the $D0_{22} \rightarrow L1_2$ and the $L1_2 \rightarrow D0_{22}$ structural changes occur in the hypo- and hyper-eutectoid regions, respectively. The features of the reaction around the eutectoid composition, $Ni_3Al_{0.1–0.4}V_{0.9–0.6}$ with $e/a = 8.70–8.55$, have been investigated experimentally and theoretically [10–13]. These studies indicate that the reaction basically proceeds by both the nucleation of the $D0_{22}$ (or $L1_2$) region at the antiphase boundary of the $L1_2$ (or $D0_{22}$) matrix and its growth in the matrix. It has also been reported that the $L1_2 + D0_{22}$ final product as an equilibrium state exhibits a checkerboard pattern, which is characterized by an alternating array of cuboidal $L1_2$ and $D0_{22}$ domains [11–13].

The above-mentioned results for the $L1_2 \Leftrightarrow D0_{22}$ structural change do not show clearly the effect of the frustrated pairwise interaction. This is because the alloys used had e/a of about 8.60, where neither structure is very stable. In order to investigate the frustration effect and its relaxation, we focused on the $L1_2 \rightarrow D0_{22}$ structural change in the $Ni_3Al_{0.52}V_{0.48}$

alloy with $e/a = 8.49$. Because this alloy is under a strongly $L1_2$-stabilized condition in terms of e/a, structural change can be expected to reveal the effect of the frustrated pairwise interaction. In this work, the change in microstructures during the $L1_2 \rightarrow D0_{22}$ structural change accompanied by fcc $\rightarrow$ $L1_2$ + $D0_{22}$ phase separation in the $Ni_3Al_{0.52}V_{0.48}$ alloy was investigated by transmission electron microscopy. As a result, spontaneous $L1_2$ single crystallization was found to occur in the alloy. This result raises an important issue that bifurcation of pattern formation appears in $Ni_3(Al, V)$ alloys. On the basis of the experimental results, the physical origin of spontaneous single crystallization and the pattern bifurcation in $Ni_3(Al, V)$ alloys will be discussed.

2. Experimental procedure

Samples of the $Ni_3Al_{0.52}V_{0.48}$ alloy were prepared in the following way. An ingot was made by an Ar-arc melting technique and annealed at 1573 K for 7 h for homogenization, followed by quenching in ice water. As will be shown later, the quenched ingot basically consisted of the $L1_2$ single phase. Samples were cut from the quenched ingot and aged at 1173 K to induce $D0_{22}$ precipitation. In order to examine the change in microstructures during the $L1_2 \rightarrow D0_{22}$ structural change, the samples were aged for 10 min and 1, 5, 10, 100 and 1000 h, followed by quenching in ice water. It should be noted that according to previous studies of the $L1_2 \rightarrow D0_{22}$ structural change in $Ni_3Al_{0.1-0.4}V_{0.9-0.6}$ alloys, samples aged for 100 h basically reach the $L1_2$ + $D0_{22}$ equilibrium state [10, 12]. Observation of the microstructure was carried out by taking electron diffraction patterns and bright- and dark-field images at room temperature using an H-800 transmission electron microscope with an accelerating voltage of 200 keV. We mainly used the electron incidence parallel to one of the $\langle 001 \rangle_{L1_2}$ directions, because the interface between the neighbouring $L1_2$ and $D0_{22}$ regions forming the checkerboard pattern is parallel to one of the $\{001\}_{L1_2}$ planes [11, 12], where the subscript $L1_2$ denotes the $L1_2$ structure. Specimens for observation were made by Ar-ion thinning after cutting the samples into discs 30 μm thick and with a 1.5 mm radius.

3. Experimental results

First of all, the features of the microstructure of the quenched sample (non-aged sample) are described. Figure 1 shows an electron diffraction pattern and corresponding bright- and dark-field images obtained from the sample. The diffraction pattern in figure 1(a) shows the coexistence of ordered spots due to the $L1_2$ structure as well as fundamental spots due to the fcc structure. In the following description, the diffraction spots are indexed in terms of the fcc structure in all diffraction patterns. It should be mentioned here that the $D0_{22}$ superlattice spots could not be detected even when the sample was rotated. This result indicates that the sample basically consisted of the $L1_2$ single phase. One feature of the diffraction patterns is that the diffraction spots are slightly elongated in the non-radial direction, as is indicated by arrow A. This elongation is indicative of the presence of small-angle tilt boundaries in the $L1_2$ single phase. In the bright-field image in figure 1(b), there exist cuboidal domains measuring about 100 nm on a side. The cuboidal domains have the $L1_2$ structure, the shape of which reflects the symmetrical nature of the crystal structure. An important feature of the image is that there exist line contrasts in one of the $\langle 100 \rangle$ directions. Based on the elongation of the diffraction spots, the dark-line contrast should be identified as the small-angle tilt boundaries, which separated into two neighbouring $L1_2$ domains. In order to examine the details of the microstructure, we took a dark-field image using a 100-ordered spot due to the $L1_2$ structure. As can be seen in

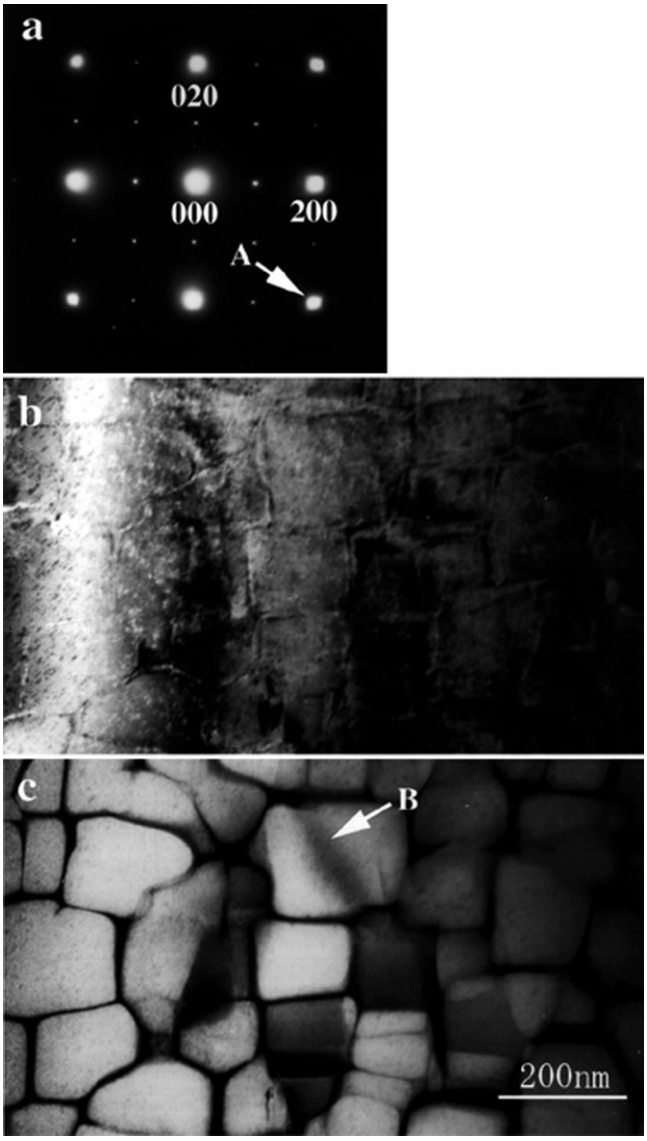

Figure 1. (a) An electron diffraction pattern, (b) a bright-field image and (c) a dark-field image obtained from a quenched sample. The diffraction spots are indexed in terms of the fcc structure. The dark-field image was taken by using a 100-ordered spot. The sample was found to consist of the $L1_2$ single phase, including both small-angle tilt boundaries and antiphase boundaries.

figure 1(c), there exist faint dark-contrast regions in the $L1_2$ domains, as indicated by arrow B, in addition to the dark-line contrast due to the small-angle tilt boundaries. The wide regions having the dark contrast were still present when the sample was rotated. This indicates that the wide dark-contrast regions must be the extended antiphase boundary. From the results mentioned above, the quenched sample was found to consist of the $L1_2$ single phase, including both the small-angle tilt boundaries and the extended antiphase boundaries.

Figure 2 shows bright- and dark-field images obtained from the sample aged for 10 min. From an analysis of the electron diffraction patterns, the sample also consisted of only the $L1_2$

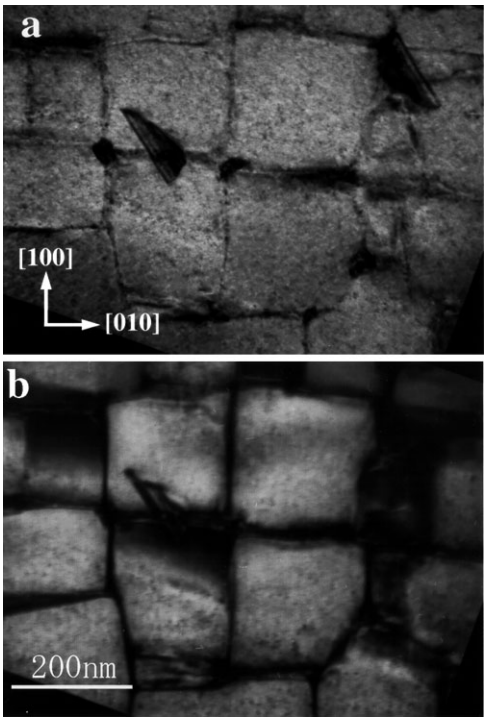

Figure 2. (a) A bright-field image and (b) a dark-field image obtained from a sample aged for 10 min. The $L1_2$ cuboidal domains became larger than those of the quenched sample, together with the annihilation of the antiphase boundaries.

single phase. In the bright-field image in figure 2(a), $L1_2$ cuboidal domains divided by the {100} boundaries are clearly observed. The boundaries were also found by analysis to be the small-angle tilt ones. The average size of the cuboidal domains was determined to be about 200 nm, which is larger than that in the quenched sample. In the dark-field image taken by using a 100-ordered spot, figure 2(b), there are fewer antiphase boundaries in the $L1_2$ domains than in the quenched sample. It is thus concluded that 10 min ageing resulted in the growth of the $L1_2$ cuboidal domains by both the migration of the small-angle tilt boundaries and the annihilation of the antiphase boundaries.

Figure 3 shows an electron diffraction pattern and corresponding bright- and dark-field images obtained from the sample aged for 1 h. In the diffraction pattern in figure 3(a), the superlattice spots due to the $D0_{22}$ structure can be detected at $1/2\ 1\ 0$-type positions in addition to the $L1_2$ ordered spots. This implies that $D0_{22}$ regions formed in the sample. A detailed analysis of the diffraction pattern indicates that the diffraction spots can be classified into three groups: two types of $D0_{22}$ spot and the $L1_2$ spots. It should be noted that the spots located at the $1/2\ 1\ 0$ (arrow A) and $1\ 1/2\ 0$ (arrow B) positions are due to two different $D0_{22}$ variants. In order to examine the features of the microstructures of the sample aged for 1 h, the bright-field image in figure 3(b) was first taken. As can be seen, there exist $L1_2$ cuboidal domains separated by small-angle tilt boundaries. However, it is hard to detect the presence of $D0_{22}$ regions. We then took dark-field images by using the $1\ 1/2\ 0$-type spots, one of which is shown in figure 3(c). It should be noted that the $1\ 1/2\ 0$ spot originates from one $D0_{22}$ variant. In the image in figure 3(c), the (010) boundaries give rise to bright contrast, although

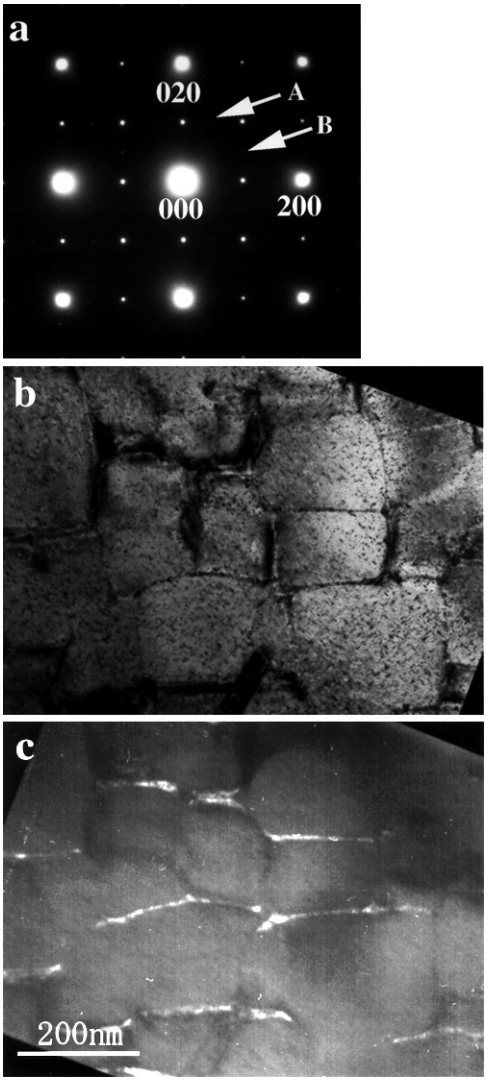

Figure 3. (a) An electron diffraction pattern and (b) and (c) dark-field images obtained from a sample aged for 1 h. The diffraction spots are indexed in terms of the fcc structure. The dark-field images in (b) and (c) were taken by using the 100- and 1/2 1 0-ordered spots, respectively. The $D0_{22}$ regions were found to nucleate at the small-angle tilt boundaries.

the (100) boundaries are observed as dark contrast. These results indicate that one $D0_{22}$ variant is nucleated along the (010) boundaries. It should be mentioned here that three $D0_{22}$ variants, respectively, formed along three $\{100\}$ boundaries. The *c*-axis of each $D0_{22}$ variant was found to be parallel to the normal of the boundary. It is therefore concluded that the $D0_{22}$ regions nucleate along the small-angle tilt boundaries of the $L1_2$ matrix in this stage.

On further ageing, changes in the microstructures take place in relation to the progress of the $L1_2 \rightarrow D0_{22}$ structural change. Figure 4 shows a bright-field image and two dark-field images obtained from the sample aged for 5 h. It should be noted that the diffraction pattern consists of two $D0_{22}$ variants and the $L1_2$ matrix in the sample, just as in the case of the sample

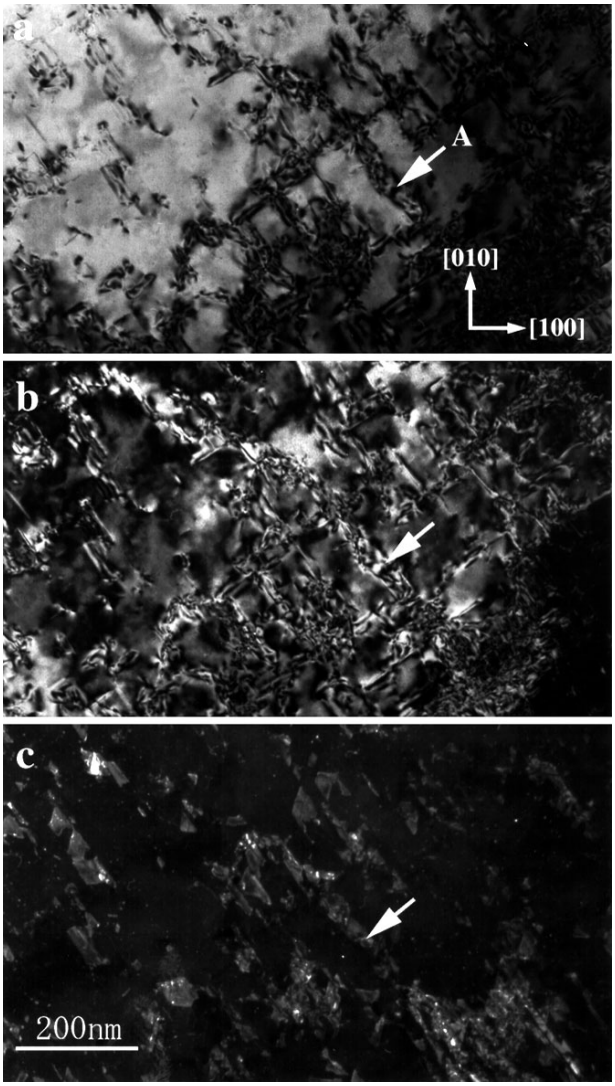

Figure 4. (a) A bright-field image and (b), (c) dark-field images of a sample aged for 5 h. The dark-field images in (b) and (c) were taken by using the 220- and 1/2 1 0-ordered spots, respectively. It was found that the direction of the $D0_{22}$ regions changed from the ⟨100⟩ to the ⟨110⟩ ones and that strong lattice strain was present at the circumference of the $D0_{22}$ regions.

aged for 1 h. In the bright-field image in figure 4(a), the $D0_{22}$ regions in the $L1_2$ matrix can be observed as indicated by arrow A. The shape of the $L1_2$ domains greatly deviates from the cuboidal shape and their average size is much larger than that in figure 3(b). Important features of the image are that the same $D0_{22}$ regions extended in one of the ⟨110⟩ directions, and that complex dark contrast is observed around the $D0_{22}$ regions. The change in their directions from the ⟨100⟩ to the ⟨110⟩ ones was caused by the misfit of the lattice parameters between the $D0_{22}$ and $L1_2$ lattices [11]. Figure 4(b) shows the dark-field image obtained by using a 220 fundamental spot. In the image, the complex strain contrast is observed in the regions that gave rise to the complex dark contrast in figure 4(a), as well as the strain contrast in the $L1_2$ matrix.

This indicates that the strain field cannot be relieved even by the change in the directions of the $D0_{22}$ extension. Figure 4(c) is a dark-field image taken by using a 1/2 1 0 superlattice spot due to the $D0_{22}$ structure. The $D0_{22}$ regions elongated in one of the ⟨110⟩ directions are actually observed as bright contrast. It should be mentioned here that the crystallographic relation and the interface between the $L1_2$ and the $D0_{22}$ regions in the checkerboard pattern are as follows: $(001)_{L1_2} \parallel (010)_{D0_{22}}$ and $\langle 110\rangle_{L1_2} \parallel \langle 101\rangle_{D0_{22}}$ and $\{110\}_{L1_2}$ plane, respectively [10, 12]. Thus the microstructure obtained in the sample aged for 5 h exhibited a transitional state to the $L1_2 + D0_{22}$ checkerboard pattern.

When the sample was kept at 1173 K for 10 h, an interesting change in the microstructure occurred. Figure 5(a) is an electron diffraction pattern obtained from the sample aged for 10 h. In the pattern, surprisingly, the diffraction spots due to the $D0_{22}$ structure vanish and only the spots due to the $L1_2$ structure are detected. This indicates that the annihilation of the $D0_{22}$ regions takes place in this stage. In the corresponding bright-field image in figure 5(b), the $D0_{22}$ regions cannot be observed at all and there exist fringe contrast regions indicating the stacking faults of the $L1_2$ matrix. The size of the $L1_2$ region is so large that the grain boundaries cannot be observed in the area shown here. In addition, no strain contrast can be detected in the $L1_2$ matrix. These results indicate that in this stage the lattice strain is released by the annihilation of the $D0_{22}$ regions, together with the growth of the $L1_2$ matrix. Figure 5(c) shows a dark-field image obtained by using a 110-ordered spot due to the $L1_2$ structure. In the image, the antiphase boundaries are clearly observed. The antiphase boundaries are basically orientated in one of the ⟨100⟩ directions. An interesting feature is that the antiphase boundaries are connected with the fringe contrast regions. From a comparison of the bright- and the dark-field images, the fringe contrast was found to be complex stacking faults, the existence of which has been known in intermetallic compounds having the $L1_2$ structure. A complex stacking fault is defined as a lattice defect having the $1/6\langle 211\rangle$-Shockley-type atomic displacement resulting from the decomposition of the superlattice dislocation and the antiphase boundary [14]. These features of the microstructure indicate that the growth of the $D0_{22}$ regions in the $L1_2$ matrix is suppressed and the bifurcation to the single $L1_2$ phase occurs in this stage.

The features of the microstructure in the sample aged for 100 h are described here. According to previous papers on $Ni_3(Al, V)$ alloys [11, 13], an ageing time of 100 h is sufficient to obtain the checkerboard pattern. The electron diffraction patterns, however, indicate that the sample consists of the $L1_2$ single phase. Figure 6 shows bright- and dark-field images of the sample. In the bright-field image in figure 6(a), only stacking faults having dark–bright–dark contrast can be observed in one of the ⟨110⟩ directions in the $L1_2$ matrix. The features of the contrast indicate that the regions correspond to complex stacking faults. In the dark-field image taken by using a 110-ordered spot due to the $L1_2$ structure, figure 6(b), there exist ⟨100⟩-directed antiphase boundaries orientated in one of the ⟨100⟩ directions as well as complex stacking faults. From the experimental results mentioned above, both the annihilation of the $D0_{22}$ regions and the single crystallization of the $L1_2$ matrix can be clearly observed in this stage. It should be mentioned that the microstructure obtained from the sample aged for 1000 h basically consisted of the single $L1_2$ phase, having a larger grain size than that of the 100 h-aged sample, and that fewer lattice defects were observed in the $L1_2$ matrix. It is therefore concluded that $L1_2$ single crystallization takes place spontaneously in the examined alloy during ageing at 1173 K.

4. Discussion

The features of the change in the microstructures of the $Ni_3Al_{0.52}V_{0.48}$ alloy during ageing at 1173 K are summarized here. The first sample observed was one consisting of single

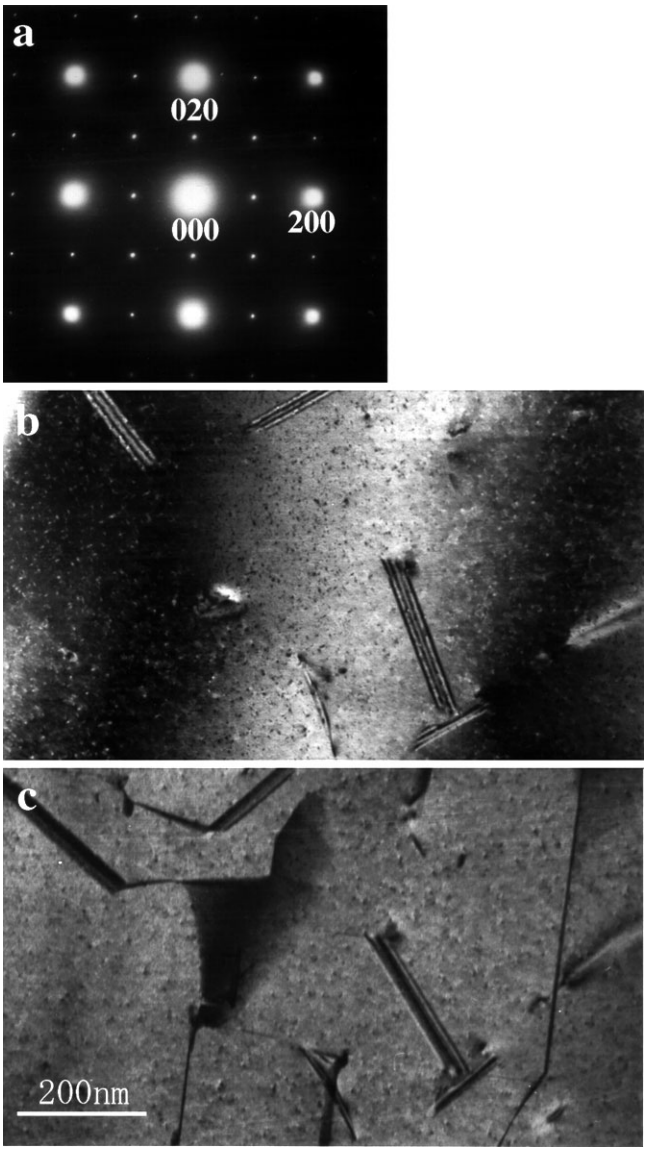

Figure 5. (a) An electron diffraction pattern, (b) a bright-field image and (c) a dark-field image obtained from a sample aged for 10 h. The dark-field image was taken by using a 110-ordered spot. The lattice strain was released by the annihilation of the $D0_{22}$ regions.

$L1_2$ regions, together with both the small-angle tilt boundaries and the extended antiphase boundaries. When samples are aged to induce the $D0_{22}$ precipitation reaction, the ⟨100⟩-directed $D0_{22}$ regions nucleate basically at the small-angle tilt boundaries. The formation of the $D0_{22}$ regions produces a strain field in the $L1_2$ matrix, resulting in a change in their directions from the ⟨100⟩ to the ⟨110⟩ ones. In spite of this, the $D0_{22}$ regions cannot grow larger and they are annihilated with further ageing. Eventually, $D0_{22}$ precipitation is suppressed and the final product is the single $L1_2$ phase, including complex stacking faults and antiphase boundaries, i.e. topological defects. This spontaneous $L1_2$ single crystallization clearly contradicts the

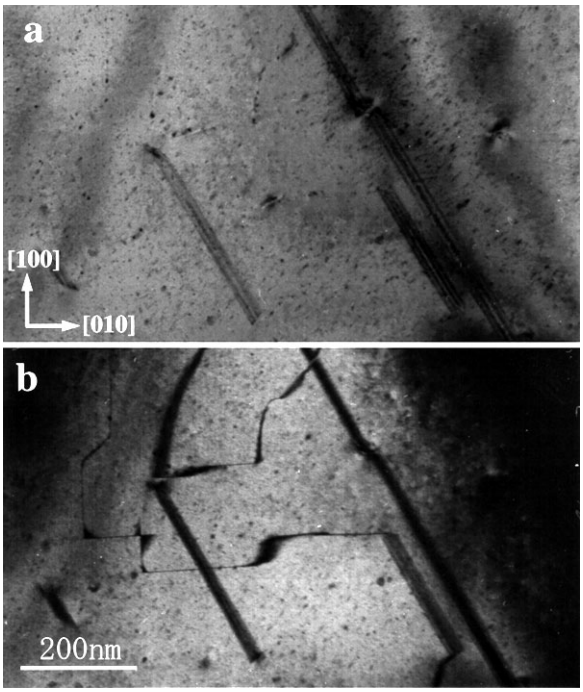

Figure 6. (a) A bright-field image and (b) a dark-field image of a sample aged for 100 h. The dark-field image was taken by using a 110-ordered spot. It was found that only large $L1_2$ grains, including lattice defects such as complex stacking faults and antiphase boundaries, were present in the sample.

microstructure expected from the phase diagram of pseudobinary Ni_3(Al, V) alloys. On the basis of the experimental results, we shall discuss here the physical origin of spontaneous single crystallization and pattern bifurcation in the alloy system.

When the alloy consisting of the initial $L1_2$ state was aged, the diffusion of V to the small-angle tilt boundaries took place in the $L1_2$ matrix and the $D0_{22}$ regions precipitated at the boundaries, accompanying the $L1_2 \rightarrow D0_{22}$ structural change. Because both structures are A_3B-type ordered structures based on the fcc lattice, the structural change basically proceeds by the rearrangement of atoms. It should be noted that the atoms present at the B sites of the ideal $L1_2$ and $D0_{22}$ structures are, respectively, Al and V, while the A-site atom of both structures is Ni. As was reported in previous papers, the nucleus of $D0_{22}$ precipitation is V present at the boundaries [11–13], and the local stress due to the presence of the small-angle tilt boundaries works to promote this precipitation. In the precipitation process, local strain induced by the misfit of the lattice parameters between the $L1_2$ and the $D0_{22}$ lattices becomes an important issue. This misfit basically originates from the difference in the atomic radius of Al (0.143 nm) and V (0.131 nm) and appears in the vicinity of the $L1_2/D0_{22}$ boundaries. In easing the misfit strain, the direction of the boundaries changes from the ⟨100⟩ to the ⟨110⟩ ones. Actually, the rotation of the boundaries accommodates the misfit strain in the alloys, in which the $L1_2$ + $D0_{22}$ checkerboard pattern finally forms [11, 13]. An important difference in the present alloy is that such accommodation cannot be achieved even by the change in the boundary direction, as was shown in figure 4. Because the $D0_{22}$ structure is characterized by the periodic array of the antiphase boundaries introduced in the $L1_2$ structure, one possible

way of dissipating the elastic energy of the misfit strain is to turn the $D0_{22}$ precipitates back to the topological defects of the $L1_2$ matrix. Thus, the $D0_{22}$ precipitates are annihilated and the $L1_2$ single phase, including topological defects, is formed, resulting in the relief of the misfit strain (see figure 5). It should be mentioned here that the final $L1_2$ state should have a smaller V concentration than the initial state due to the segregation of V at the defects. A comparison of the final and the initial $L1_2$ states shows that many small-angle tilt boundaries disappear and the concentration deviation from the stoichiometry of the $L1_2$ structure (e/a: 8.25) becomes smaller in the final state. It is obvious that the free energy of the final state becomes lower than that of the initial state in terms of both the elastic and the atomic configuration energies.

Let us simply discuss the bifurcation of the final pattern of the $L1_2 \rightarrow D0_{22}$ structural change in $Ni_3(Al, V)$ alloys. The misfit strain appearing in the vicinity of the $L1_2/D0_{22}$ boundaries becomes a key factor for the final pattern formation. Concretely, the accommodation of the misfit strain results in the formation of the $L1_2 + D0_{22}$ checkerboard pattern, while the $L1_2$ single phase containing topological defects forms due to an inability to accommodate the strain. It is proposed here that frustration plays a crucial role in determining whether such accommodation is achieved or not. When the V concentration in the $L1_2$ matrix is small, the matrix is under a strongly $L1_2$-stabilized condition and the degree of frustration becomes larger. It should be mentioned here that the V concentration of the present alloy is smaller than that of the alloys in which the formation of the $L1_2 + D0_{22}$ checkerboard pattern has been found. In order to relieve such frustration, locally disordered states should form as buffer regions around the $L1_2/D0_{22}$ boundaries, but the formation of such regions induces local strain there. This indicates that the reduction of frustration raises the elastic energy due to the appearance of the buffer regions. Alloys having a large V concentration, on the other hand, do not have an $L1_2$-stabilized atomic configuration. Such alloys do not produce large frustration and the buffer regions are not necessary in promoting the $L1_2 \rightarrow D0_{22}$ structural change. Thus, accommodation of the misfit strain can be accomplished by the rotation of the $L1_2/D0_{22}$-boundary direction and the final state becomes the $L1_2 + D0_{22}$ state.

On the basis of the foregoing discussion, the strain field appearing in the vicinity of the $L1_2/D0_{22}$ boundaries directly controls the pattern bifurcation related to the $L1_2 \rightarrow D0_{22}$ structural change in pseudobinary $Ni_3(Al, V)$ alloys. The achievement of strain accommodation depends on the degree of the concentration deviation in the initial $L1_2$ matrix from the equilibrium $L1_2$ state. It is concluded that the spontaneous single $L1_2$ crystallization found in the $Ni_3Al_{0.52}V_{0.48}$ alloy originates from an inability to accommodate misfit strain. That inability is triggered by strong frustration due to the small concentration deviation from the stoichiometric $L1_2$ composition.

Acknowledgment

The authors would like to thank Mr A Hirata, Waseda University, for his technical support in this work.

References

[1] Chung I, Durrer R, Turok N and Yurke B 1991 *Science* **251** 1336
[2] Runnels L K 1972 *Phase Transition and Critical Phenomena* vol 2, ed C Domb and M S Green (New York: Academic)
[3] Kanamori J 1966 *Prog. Theor. Phys.* **35** 16
[4] Kaburagi M and Kanamori J 1975 *Prog. Theor. Phys.* **54** 30
[5] Tanimura M, Inoue Y and Koyama Y 1995 *Phys. Rev.* B **52** 15 239
Tanimura M, Inoue Y and Koyama Y 1997 *Phys. Rev.* B **55** 14 063

Tanimura M, Inoue Y and Koyama Y 1998 *Mater. Trans. JIM* **39** 57
Tanimura M, Inoue Y and Koyama Y 2001 *Scr. Mater.* **44** 365
[6] Bhatt R N 1977 *Phys. Rev.* B **16** 1915
[7] Liu C T and Stiegler J O 1984 *Science* **226** 636
[8] Lin W, Xu J-H and Freeman A J 1992 *Phys. Rev.* B **45** 10 863
[9] Cabet E, Pasturel A, Ducastelle F and Loiseau A 1996 *Phys. Rev. Lett.* **76** 3140
[10] Hong T M, Mishima Y and Suzuki T 1988 *MRS Symp. Proc.* **133** 429
[11] Takeyama M and Kikuchi M 1998 *Intermetallics* **6** 573
[12] Wang Y, Chen L-Q and Khachaturyan A G 1993 *Acta. Metall. Mater.* **41** 279
[13] Poduri R and Chen L-Q 1998 *Acta. Mater.* **46** 1719
[14] Kear B H and Wilsdorf H G F 1962 *Trans. Met. Soc. AIME* **224** 382